A Single Closed-Loop Kinematic Chain Approach for a Hybrid Control of Two Cooperating Arms with a Passive Joint: An Application to Sawing Task

Hee-Joo Yeo, Il Hong Suh, *Member, IEEE,* Byung-Ju Yi, *Member, IEEE,* and Sang-Rok Oh, *Member, IEEE*

***Abstract*—This work deals with a sawing task performed by two cooperating arms. The two-arm system under our hand consists of a four degree-of-freedom (DOF) SCARA robot and a five DOF PT200V robot. When the two arms are rigidly grasping a saw, the mobility of the system is three, which is not enough for sawing tasks. Therefore, we deliberately insert a passive joint at the end of the SCARA robot to increase the mobility up to four.**

A hybrid control method to regulate the force and velocity by the two arms is proposed in this work. The proposed scheme has three typical features; first, the two arms are treated as one arm in a kinematic viewpoint. Secondly, our approach is different from other acceleration-based approach, in the sense that our hybrid control method is based on a Jacobian and an internal kinematics for a single closed-kinematic chain of the two arms to reflect the nature of the position-controlled industrial manipulator. Thirdly, the proposed scheme is not only able to operate the system even if a passive joint exists, but also is able to utilize the internal loads for useful applications such as pitch motion control. We experimentally show that the performance of the velocity and force response are satisfactory, and that one additional passive joint not only prevents the system from unwanted roll motion in the sawing task, but also allows an unwanted pitch motion to be notably reduced by an internal load control. To show the effectiveness of the proposed algorithms, we perform experimentation under several, different conditions for saw, such as three saw blades, two sawing speeds, and two vertical forces.

***Index Terms*— Closed-chain mechanism, compliance control, cooperating arms, dual arms, force control, hybrid control, internal force (or load) control, redundant actuation, sawing task.**

I. Introduction

MANY tasks for industry automation require manipulators to interact with the environment. Basic examples of those tasks include sawing, pushing/pulling, scraping, grinding, pounding, polishing, bending, and twisting. All of such tasks intrinsically require that manipulators be both position- and force-controlled.

Many of current industrial robot manipulators are position-controlled devices. This implies that the force cannot be directly controlled by actuators, but is indirectly controlled by measuring the force error and compliantly adjusting the end-position of the manipulator. The so-called, compliance control schemes [1], [9], [12], [13], [18], [29] have been employed in the control of a single robot in contact with its environment. Most works on this subject led to the introduction of the hybrid position/force control system [2], [10], [14]–[16], [22], [30]. Basic examples of those tasks include scraping, grinding, polishing, and sawing.

Multiple cooperating robots can perform many tasks which cannot be carried out by using a single arm. These tasks include the handling of heavy and large objects, and assembly of complex parts or part mating, and so on. Multiple arms or dual arms can be described as a force-redundant system, since these systems possess more actuators than the system's mobility. Therefore, force redundancy raises the force-distribution problem among the arms. The force distribution problem can be categorized as two subjects; load sharing and load balancing. Dynamic loads and external loads applied to a grasped object held by the multiple arms can be evenly distributed to (or shared by) each arm according to some criteria [10], [12], [14], [22], [23], [29], [30]. Internal force does not influence the motion of the system, but balances the system. It can be beneficially utilized to squeeze, bend, and shear the object grasped by the arms or internally generate a stiffness effect in a feedforward fashion [3], [5], [11], [17], [26]–[28].

As control methods for multiple arms, master/slave scheme and nonmaster/slave scheme have been proposed. Tao and Luh *et al.* [9] considered a compliant coordination control of two robots employing a master/slave scheme. Their application was an assembly operation between a bolt and nut. Kosuge *et al.* [18] proposed a decentralized control scheme of dual arms. To execute the task in a decentralized way, the motion of the object is given to the leader, and the follower estimates the motion of the leader based on the information from its own force sensors. However, it has been known from the previous practices that the master/slave approach suffers from time delay in force tracking, because knowledge of the desired position is only accessible for the master, and that this scheme does not actually represent load distribution between two arms. In order to overcome these drawbacks, Fujii and Kurono [20] have proposed a nonmaster/slave scheme. Their method first defines position/orientation reference to the object, from which position/orientation references to the hands of the two

Manuscript received May 30, 1997; revised October 26, 1998. This paper was recommended for publication by Associate Editor N. Kirkansei and Editor A. Goldenberg upon evaluation of the reviewers' comments.

H.-J. Yeo is with the Department of Electronics Engineering, Daejin University, Kyungki-Do 487-711, Korea.

I. H. Suh and B.-J. Yi are with Hanyang University, Kyungki-Do 425-791, Korea.

S.-R. Oh is with the Intelligent System Control Research Center, Korea Institute of Science and Technology, Seoul 136-130, Korea.

Publisher Item Identifier S 1042-296X(99)00992-1.

robots are calculated. Next, they introduced a compliance control technique for the coordination of the two robots. By introducing the technique, however, they lost the positioning accuracy of the object. To resolve this problem, Uchiyama *et al.* [22] proposed a symmetric hybrid position/force control scheme for the coordination of two arms. Here, their scheme is symmetric in the sense that the workspace vectors defined are symmetric functions of the joint space vectors of the two robots. In their scheme, two arms equipped with force/torque sensors at each wrist simultaneously regulate force and position. Bonitz and Hsia [21] proposed an internal force-based impedance control for cooperating two arms. Their algorithm was successfully applied to the internal force control for the grasped object. However, previous works on multiple arms have treated only parallel manipulators that consist of several identical manipulators. Also, the case that some of the joint actuators of multiple arms are not activated has not been considered yet.

In this work, we propose a hybrid control method for a sawing task using two arms. The proposed scheme has three typical features; first, the two arms are treated as one arm in a kinematic viewpoint. This approach is quite useful when dealing with the kinematics, dynamics, and control of a two-arm system with general kinematic structure. Secondly, our approach is different from other acceleration-based approaches in the sense that our hybrid control method is based on a Jacobian and an internal kinematics for a single closed-kinematic chain of the two arms to reflect the nature of the position-controlled industrial manipulator. Thirdly, the proposed scheme is not only able to operate the system even if a passive joint exists, but also able to utilize the internal loads for useful applications such as pitch motion control. Our two-arm system consists of a four degree-of-freedom (DOF) SCARA robot and a five DOF PT200 robot. In order to estimate the degree-of-motion for any robotic system, we need to evaluate the mobility of such system. Here, the mobility of a manipulator is equal to the number of independent variables which can be specified to locate all members of the mechanism relative to one another. However, the mobility of our system is three, which is not enough to control three positional variables and one force variable. Therefore, in order to increase the mobility of the system up to four, we deliberately insert a passive joint at the end of the SCARA robot. We experimentally show that the performance of the velocity and force response are satisfactory, and that one additional passive joint not only prevents the system from unwanted roll motion in the sawing task, but also allows an unwanted pitch motion to be notably reduced by an internal load control.

This paper is organized as follows. Initially, in Section II, a typical feature of a sawing task by two cooperating arms is described. Next, in Section III, we introduce a kinematic modeling methodology for general two-arm configurations. Force control and velocity control algorithms for a sawing task are presented in Sections IV and V, respectively. In Section VI, experimental results to corroborate the proposed control scheme are presented. Finally, in Section VII, we draw conclusions.

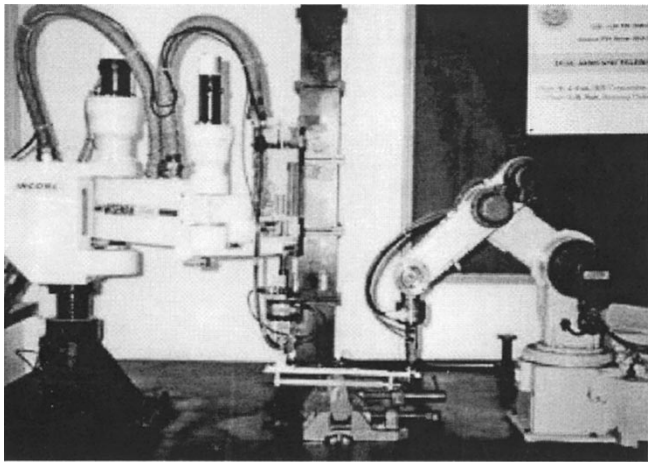

Fig. 1. Experimental setup for sawing task.

II. Sawing Task by Two Cooperating Arms

In the sawing task, the trajectory of the saw grasped by the two arms is first planned in an off-line fashion. When the trajectory is planned to follow a line in a horizontal plane, three directional motions have to be controlled (i.e., two translational motions and one rotational motion). Also, a certain level of force has to be controlled toward the vertical direction (i.e., minus z-direction) not to loose the contact with the object to be sawn. A typical feature of the sawing task is that the contact position is continuously changing. Therefore, the kinematic mapping between the force-controlled position and the joint actuators has to be updated continuously.

Fig. 1 represents our two-arm system which consists a four DOF SCARA robot and a five DOF PT200 robot. Assume that J, L, F_i, and C denote the numbers of joints, links, DOF of each joint, and the maximum DOF of each link (six for spatial motion and three for planar or spherical motion), respectively. Then, according to the mobility equation, given by [31]

$$D = C(L-1) - \sum_{i=1}^{J}(C - F_i) \tag{1}$$

the mobility of our two-arm system is three where the two arms are rigidly grasping a saw. Since it is not enough to control three positional variables and one force variable, we deliberately insert a passive revolute joint at the end of the SCARA robot such that the direction of the axis is parallel to the y axis of the saw coordinate system, as shown in Fig. 2, to increase the mobility of the system up to four. In our experiment, we demonstrate that the additional passive joint plays an important role.

III. Kinematic Modeling of Two Arms

The kinematics of general closed-chain systems such as multiple arms or dual arms is divided into two layers [11]. The first layer describes the internal relationship between the *independent* joint set and the *dependent* joint set. The kinematic relationship is obtained by relating higher-order kinematic constraint equations among the multiple chains.

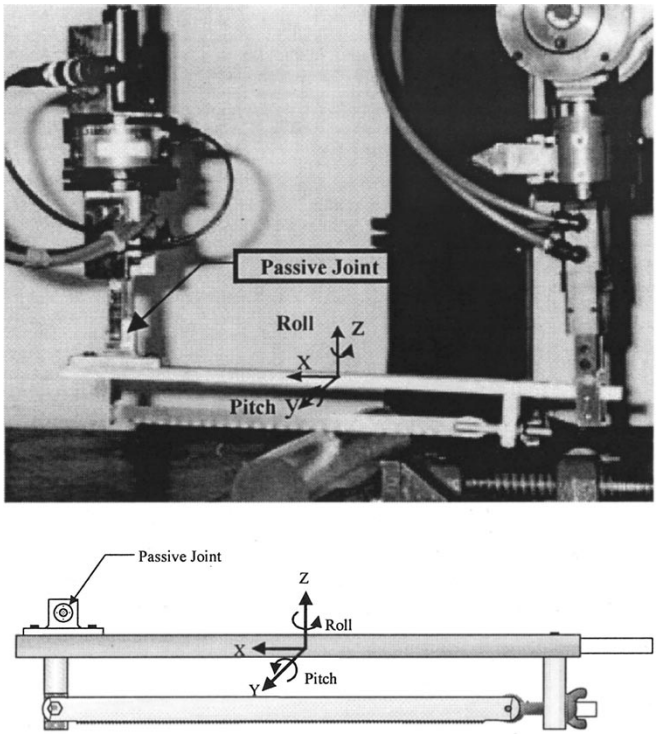

Fig. 2. A passive joint and the saw.

The second layer deals with relationship between the end-effector motion coordinates and the independent set of actuator coordinates. This mapping is obtained by embedding internal kinematic relationships determined from the first layer, into the model of an open-chain kinematic relation.

A. Internal Kinematics

The following discusses internal kinematics of dual arms which consist of two serial chains connected to (or holding) a common object moving in a N-dimensional operation space. Each chain may have different number of joints. Since each arm has a common higher-order kinematics such as velocity and acceleration at the end-effector coordinate, the end-effector coordinate is here chosen as an intermediate coordinate set to determine the internal kinematic relationship.

The velocity vector of the end-effector $(\dot{\boldsymbol{u}})$ can be expressed directly in terms of the joint velocity vector $({}_{\boldsymbol{r}}\dot{\boldsymbol{\phi}})$ of the rth open-chain structure, according to

$$\dot{\boldsymbol{u}} = [{}_{\boldsymbol{r}}\boldsymbol{J}]_{\boldsymbol{r}}\dot{\boldsymbol{\phi}} \qquad r = 1, 2 \tag{2}$$

where $[{}_rJ]$ denotes the first-order kinematic influence coefficient (KIC) matrix (or Jacobian) relating the end-effector coordinate vector to the joint coordinate vector. Equation (2) implies that there are N algebraic equations relating one of the joint velocity set to the other set. This can be expressed as

$$[{}_1\boldsymbol{J}]_1\dot{\boldsymbol{\phi}} = [{}_2\boldsymbol{J}]_2\dot{\boldsymbol{\phi}}. \tag{3}$$

Now, (3) can be rearranged and regrouped according to the independent and dependent coordinate velocity sets of each chain as

$$[{}_1\boldsymbol{J_a}]_1\dot{\boldsymbol{\phi}}_{\boldsymbol{a}} + [{}_1\boldsymbol{J_p}]_1\dot{\boldsymbol{\phi}}_{\boldsymbol{p}} = [{}_2\boldsymbol{J_a}]_2\dot{\boldsymbol{\phi}}_{\boldsymbol{a}} + [{}_2\boldsymbol{J_p}]_2\dot{\boldsymbol{\phi}}_{\boldsymbol{p}}. \tag{4}$$

Then, (4) is augmented into single matrix equation, given by

$$[\boldsymbol{A}]\dot{\boldsymbol{\phi}}_{\boldsymbol{p}} = [\boldsymbol{B}]\dot{\boldsymbol{\phi}}_{\boldsymbol{a}} \tag{5}$$

where

$$[\boldsymbol{A}] = [[{}_1J_p] - [{}_2J_p]] \tag{6}$$

and

$$[\boldsymbol{B}] = [-[{}_1J_a]\,[{}_2J_a]]. \tag{7}$$

Assume that M_r denotes the number of joint (or mobility) of rth open-chain. Then, in (4) and (5), $\dot{\boldsymbol{\phi}}_{\boldsymbol{a}}$ and $\dot{\boldsymbol{\phi}}_{\boldsymbol{p}}$, respectively, denotes the M dimensional independent joint velocity vector and the $\boldsymbol{N}(= \boldsymbol{M}_1 + \boldsymbol{M}_2 - \boldsymbol{M})$ dimensional dependent joint velocity vector. The subscripts a and p denote the *independent* and *dependent* coordinates, respectively. $[\boldsymbol{A}]$ and $[\boldsymbol{B}]$ implies the $\boldsymbol{N} \times \boldsymbol{N}$ and $\boldsymbol{M} \times \boldsymbol{M}$ matrices, respectively.

Therefore, direct inversion of the square matrix $[\boldsymbol{A}]$, which is assumed to be nonsingular [32], gives

$$\dot{\boldsymbol{\phi}}_{\boldsymbol{p}} = [\boldsymbol{A}]^{-1}[\boldsymbol{B}]\dot{\boldsymbol{\phi}}_{\boldsymbol{a}} = [\boldsymbol{G}_{\boldsymbol{a}}^{\boldsymbol{p}}]\dot{\boldsymbol{\phi}}_{\boldsymbol{a}} \tag{8}$$

where $[\boldsymbol{G}_{\boldsymbol{a}}^{\boldsymbol{p}}]$ of dimension $\boldsymbol{N}\times\boldsymbol{M}$ denotes the first-order internal kinematic influence coefficient $(IKIC)$ matrix of the dual arm system. Assuming that $\boldsymbol{\phi}$ represents the whole joint set of the system, the relationship between the independent joint set and the whole joint set is expressed as

$$\dot{\boldsymbol{\phi}} = [\boldsymbol{G}_{\boldsymbol{a}}^{\boldsymbol{\phi}}]\dot{\boldsymbol{\phi}}_{\boldsymbol{a}} \tag{9}$$

where $[\boldsymbol{G}_{\boldsymbol{a}}^{\boldsymbol{\phi}}]$ of dimension $\boldsymbol{M_t}(= \boldsymbol{N} + \boldsymbol{M}) \times \boldsymbol{M}$ is obtained as below

$$[G_a^{\phi}] = \begin{bmatrix} [I] \\ [G_a^{p}] \end{bmatrix}. \tag{10}$$

B. Forward Kinematics

Since joints of the rth chain $({}_{\boldsymbol{r}}\boldsymbol{\phi})$ are composed of some of the independent and dependent joints, ${}_{\boldsymbol{r}}\dot{\boldsymbol{\phi}}$ can be expressed in terms of the independent joints of the system as given by

$${}_{\boldsymbol{r}}\dot{\boldsymbol{\phi}} = \begin{bmatrix} {}_{\boldsymbol{r}}\dot{\boldsymbol{\phi}}_{\boldsymbol{a}} \\ {}_{\boldsymbol{r}}\dot{\boldsymbol{\phi}}_{\boldsymbol{p}} \end{bmatrix} = [{}_{\boldsymbol{r}}\boldsymbol{G}_{\boldsymbol{a}}^{\boldsymbol{\phi}}]\dot{\boldsymbol{\phi}}_{\boldsymbol{a}} \tag{11}$$

where $[{}_r\boldsymbol{G}_{\boldsymbol{a}}^{\boldsymbol{\phi}}]$ is obtained by augmenting the elements of (8) into ${}_{\boldsymbol{r}}\dot{\boldsymbol{\phi}}_{\boldsymbol{p}}$. Thus, the forward kinematics for the common object is finally obtained by plugging the first-order IKIC into one of the open-chain kinematic expressions as follows:

$$\dot{\boldsymbol{u}} = [{}_{\boldsymbol{r}}\boldsymbol{J}]_{\boldsymbol{r}}\dot{\phi} = [\boldsymbol{G}_{\boldsymbol{a}}^{\boldsymbol{u}}]\dot{\phi}_{\boldsymbol{a}} \tag{12}$$

where

$$[\boldsymbol{G}_{\boldsymbol{a}}^{\boldsymbol{u}}] = [{}_{\boldsymbol{r}}\boldsymbol{J}][{}_{\boldsymbol{r}}\boldsymbol{G}_{\boldsymbol{a}}^{\boldsymbol{\phi}}]. \tag{13}$$

It is remarked that the methodology introduced in this section can be applied not only to two arms but also to general multiple arms.

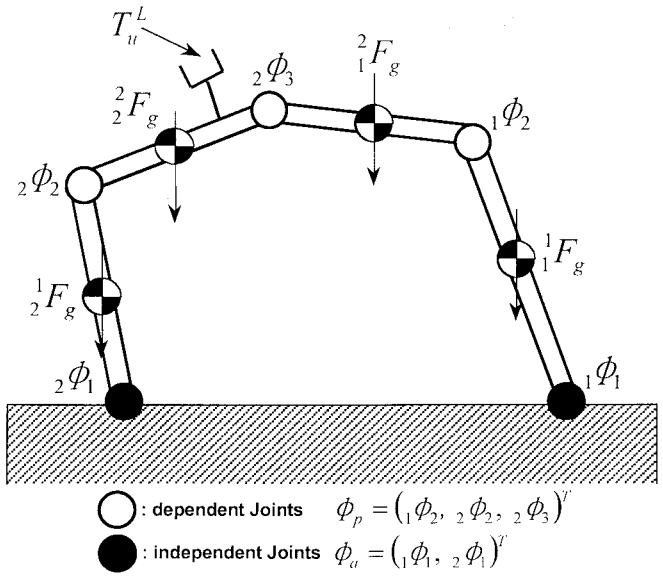

Fig. 3. Closed-loop kinematic chain.

IV. Force Control Algorithm for Sawing Task

A. Compliance Modeling

In this section, a general compliance model for a general two-arm system is developed and it is applied to the force control in the sawing task. In the sawing task, a certain level of force has to be controlled toward the vertical direction (i.e., minus z-direction) not to loose the contact with the object to be sawn.

Note that the dimensions of $\dot{\boldsymbol{u}}$ and $[\boldsymbol{G}_{\boldsymbol{a}}^{\boldsymbol{u}}]$ are 6×1 and 6×4, respectively, in three-dimensional space. Since only the force along the z-direction is controlled in the sawing task, a Jacobian which relates the force vector, $\delta \boldsymbol{F}$, to the joint minimum actuators is given as

$$\boldsymbol{\delta T_a} = [\boldsymbol{J}_1]^{\boldsymbol{T}} \boldsymbol{\delta F} \tag{14}$$

where $[\boldsymbol{J}_1]$ denotes a matrix of dimension of 1×4, which is the third rows of $[\boldsymbol{G}_{\boldsymbol{a}}^{\boldsymbol{u}}]$. Note that the force control in the sawing task is different from those in previous works [2], [6], [14], [21], [22], in that the contact position is continuously changing. We resolve this problem by continuously updating the kinematic mapping $[\boldsymbol{J}_1]$ according to the position information of the system.

The dynamics of a general closed-chain manipulator can be represented in terms of a minimum (independent) coordinate set being equal in number to the minimum number of inputs (i.e., mobility) required to completely describe the system kinematics. Consider a closed-loop kinematic chain shown in Fig. 3.

Assume that the system is in a state of equilibrium. Then, the effective load $\boldsymbol{T}_{\boldsymbol{a}}^{*}$ referenced to the independent joints, which is described in terms of the system's effort sources ($\boldsymbol{T_a}$ and $\boldsymbol{T_p}$), externally applied loads ($\boldsymbol{T}_{\boldsymbol{u}}^{\boldsymbol{L}}$), and effective gravity loads ($\boldsymbol{T}_{\boldsymbol{\phi}}^{\boldsymbol{G}}$) as follows, must be zero, that is

$$\boldsymbol{T}_{\boldsymbol{a}}^{*} = [\boldsymbol{G}_{\boldsymbol{a}_1}^{\phi}]^{\boldsymbol{T}} \boldsymbol{T}_{\phi} - [\boldsymbol{J}_1]^{\boldsymbol{T}} \boldsymbol{T}_{\boldsymbol{u}}^{\boldsymbol{L}} + [\boldsymbol{G}_{\boldsymbol{a}_1}^{\phi}]^{\boldsymbol{T}} \boldsymbol{T}_{\phi}^{\boldsymbol{G}} = 0 \tag{15}$$

where $[\boldsymbol{G}_{a_1}^{\phi}]$ denotes the matrix excluding the row corresponding to the additional passive joint from $[\boldsymbol{G}_{a}^{\phi}]$, since the passive joint cannot be activated, and we define

$$\boldsymbol{T}_{\phi} = \begin{bmatrix} \boldsymbol{T_a} \\ \boldsymbol{T_p} \end{bmatrix} \tag{16}$$

$$\boldsymbol{T}_{\boldsymbol{a}}^{*} = [\boldsymbol{G}_{\boldsymbol{a}_1}^{\phi}]^{\boldsymbol{T}} \boldsymbol{T}_{\phi}^{*} \tag{17}$$

$$\boldsymbol{T}_{\phi}^{*} = [({}_1\boldsymbol{T}_{\phi}^{*})^{\boldsymbol{T}} ({}_2\boldsymbol{T}_{\phi}^{*})^{\boldsymbol{T}}]^{\boldsymbol{T}} \tag{18}$$

$$\boldsymbol{T}_{\phi}^{\boldsymbol{G}} = [({}_1\boldsymbol{T}_{\phi}^{\boldsymbol{G}})^{\boldsymbol{T}} ({}_2\boldsymbol{T}_{\phi}^{\boldsymbol{G}})^{\boldsymbol{T}}]^{\boldsymbol{T}} \tag{19}$$

and

$${}_{\boldsymbol{r}}\boldsymbol{T}_{\phi}^{\boldsymbol{G}} = \sum_{\boldsymbol{i}=1}^{\boldsymbol{M}_i} [{}_{\boldsymbol{r}}^{\boldsymbol{i}}\boldsymbol{G}_{\phi}^{\boldsymbol{c}}]^{\boldsymbol{T}} {}_{\boldsymbol{r}}^{\boldsymbol{i}}\boldsymbol{F}_{\boldsymbol{G}} \quad r = 1, 2. \tag{20}$$

The inertial load and gravity loads, referenced to the independent input set, are obtained from the open-chain dynamics via a virtual work-based transfer method employing $[\boldsymbol{G}_{\boldsymbol{a}}^{\phi}]$. $\boldsymbol{T_a}$ and $\boldsymbol{T_p}$ denote the efforts of the independent and dependent joints, respectively. $\boldsymbol{T}_{\phi}$ denotes the effort of the total joints. $\boldsymbol{T}_{\boldsymbol{u}}^{\boldsymbol{L}}$ is an external load applied to the object coordinated u. ${}_{\boldsymbol{r}}^{\boldsymbol{i}}\boldsymbol{F}_{\boldsymbol{G}}$ is the gravity load acting on the center of gravity of the ith link of the rth chain and ${}_{\boldsymbol{r}}\boldsymbol{T}_{\phi}^{*}$ and ${}_{\boldsymbol{r}}\boldsymbol{T}_{\phi}^{\boldsymbol{G}}$ are the total effective inertial and gravity loads of the rth chain referenced to the inputs of the rth chain, respectively. The matrix $[{}_{r}^{i}\boldsymbol{G}_{\phi}^{c}]$ is the Jacobian that relates the mass center of the ith link of the rth chain to the inputs of the rth chain.

Assuming that only minimum actuators are activated, (15) can be equivalently expressed as

$$\boldsymbol{T_a} = [\boldsymbol{J}_1]^{\boldsymbol{T}} \boldsymbol{T}_{\boldsymbol{u}}^{\boldsymbol{L}} - [\boldsymbol{G}_{\boldsymbol{a}_1}^{\phi}]^{\boldsymbol{T}} \boldsymbol{T}_{\phi}^{\boldsymbol{G}} \tag{21}$$

and a linearized form of (21) is obtained as

$$\begin{aligned} \delta T_a = {} & [J_1]^T \delta(T_u^L) + (T_u^L)^T \circ \left[\frac{\partial [J_1]^T}{\partial \phi_a} \delta \phi_a \right] \\ & - [G_{a_1}^{\phi}]^T \delta(T_{\phi}^G) - (T_{\phi}^G)^T \circ \left[\frac{\partial [G_{a_1}^{\phi}]^T}{\partial \phi_a} \delta \phi_a \right] \end{aligned} \tag{22}$$

where the symbol "$\circ$" denotes a generalized scalar dot product [11] which is useful in the product of a three-dimensional array and a vector.

Given an external disturbance to the system, the resulting behavior can now be modeled as a spring action with respect to independent inputs of the system. Thus, the system stiffness equation is obtained by differentiating both sides of (22) with respect to ϕ_a as follows [11]:

$$\begin{aligned} [\boldsymbol{K_{aa}}] = {} & -\frac{\partial \boldsymbol{T_a}}{\partial \boldsymbol{\phi_a}} \\ = {} & [\boldsymbol{J}_1]^{\boldsymbol{T}} [\boldsymbol{K_{uu}}] [\boldsymbol{J}_1] - \boldsymbol{T_u} \frac{\partial [\boldsymbol{J}_1]^{\boldsymbol{T}}}{\partial \boldsymbol{\phi_a}} \\ & - [\boldsymbol{G}_{\boldsymbol{a}_1}^{\phi}]^{\boldsymbol{T}} [\boldsymbol{V}] [\boldsymbol{G}_{\boldsymbol{a}_1}^{\phi}] + \boldsymbol{T}_{\phi}^{\boldsymbol{G}} \frac{\partial [\boldsymbol{G}_{\boldsymbol{a}_1}^{\phi}]^{\boldsymbol{T}}}{\partial \boldsymbol{\phi_a}} \end{aligned} \tag{23}$$

since the following actions hold:

$$\delta T_a = -[K_{aa}] \delta \phi_a, \tag{24}$$

$$\delta T_u^L = -[K_{uu}] \delta u, \quad \text{and} \tag{25}$$

$$\delta T_{\phi}^G = -[V] \delta \phi \tag{26}$$

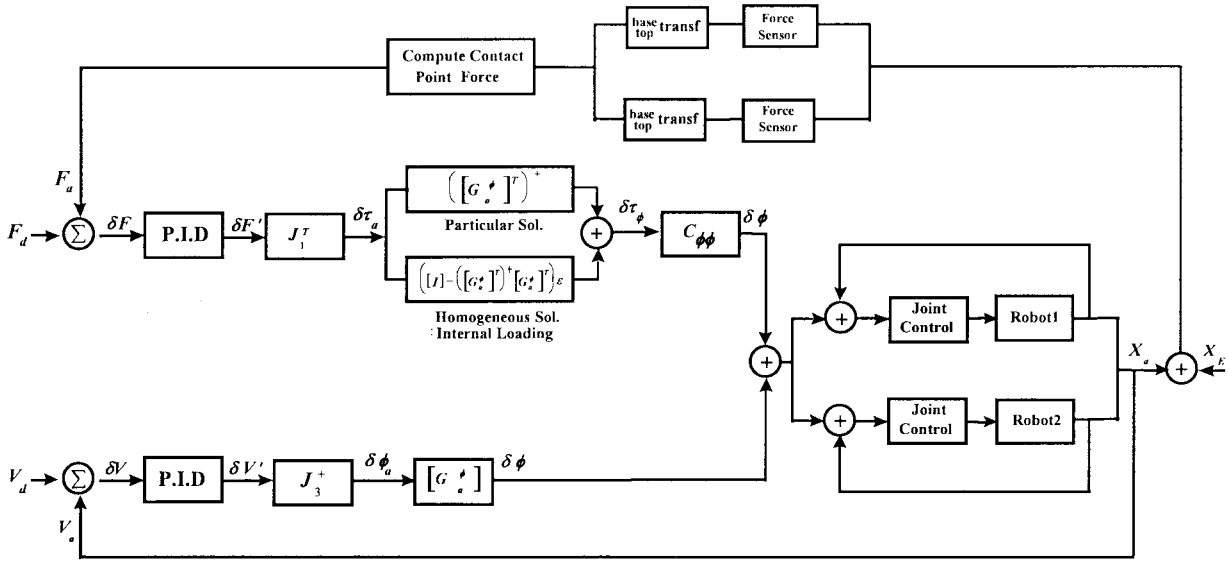

Fig. 4. Block diagram of the proposed hybrid control scheme.

where $[V]$ is a $M_t \times M_t$ block diagonal matrix, each block diagonal element of which is given by

$$[\boldsymbol{V_r}] = \sum_{i=1}^{M_i} \frac{\partial [{}^{i}_{r}\boldsymbol{G}^{c}_{\phi}]^{T}}{\partial_{r}\phi} ({}^{i}_{r}\boldsymbol{F_G}), \qquad r = 1, 2. \tag{27}$$

The second term, and the third and fourth term of the right-side of (23) denote additional stiffness effects due to the external applied loads and gravity loads, respectively. On the other hand, a compliance matrix referenced to the minimum input can be expressed as

$$[\boldsymbol{C_{aa}}] = [\boldsymbol{K_{aa}}]^{-1}. \tag{28}$$

In the case of full actuation, the effective effort at the minimum actuator site is given by

$$\boldsymbol{T_a} = [\boldsymbol{G^{\phi}_a}]^{\boldsymbol{T}} \boldsymbol{T}_{\phi} \tag{29}$$

with the differential relation expressed as

$$\delta \boldsymbol{T_a} = [\boldsymbol{G^{\phi}_a}]^{\boldsymbol{T}} \delta \boldsymbol{T}_{\phi}. \tag{30}$$

For an infinitesimal motion, the equivalent kinematic model of (9) is given by

$$\delta\phi = [\boldsymbol{G^{\phi}_a}] \delta\phi_{\boldsymbol{a}}. \tag{31}$$

Here, $\delta\phi$ and $\delta\phi_a$ can be represented by the following relations:

$$\delta\phi = -[\boldsymbol{C}_{\phi\phi}] \delta \boldsymbol{T}_{\phi} \tag{32}$$

where $[C_{\phi\phi}]$ represents the compliance matrix for total actuator coordinates and

$$\delta\phi_{\boldsymbol{a}} = -[\boldsymbol{C_{aa}}] \delta \boldsymbol{T_a}. \tag{33}$$

Substituting (30) into (33), and (32) and (33) into (31) yields a compliance relationship between the total actuator coordinates and the minimum actuator coordinates given as

$$[C_{\phi\phi}] = [G^{\phi}_{a_1}][C_{aa}][G^{\phi}_{a_1}]^{T}. \tag{34}$$

For a very hard environment, the stiffness $[\boldsymbol{K_{uu}}]$ of the environment is very large compared to the additional stiffness effects due to the externally applied force, gravity loads, and joint loads as seen from (23), therefore (34) can be simplified as

$$[C_{\phi\phi}] = [G^{\phi}_{a}][J_1]^{+}[K_{uu}]^{-1}([J_1)^{+})^{T}[G^{\phi}_{a}]^{T} \tag{35}$$

where $[\boldsymbol{J}_1]^{+}$ and $([\boldsymbol{J}_1]^{T})^{+}$ denote the pseudo-inverse solutions of $[\boldsymbol{J}_1]$ and $[\boldsymbol{J}_1]^{T}$, respectively, and the dimension of $[\boldsymbol{K_{uu}}]$ in the sawing task is 1 by 1 (i.e., scalar), since the force control is only along the z-direction.

B. Force Control Algorithm

Fig. 4 represents a block diagram of the proposed controller. A simple PID force controller [33] is employed to compensate for the force error and thus maintain a good force response. Then, for the compensated force error $\delta \boldsymbol{F'}$, the effort $(\delta \boldsymbol{T_a})$ at the minimum input locations is computed as

$$\delta \boldsymbol{T_a} = [\boldsymbol{J}_1]^{\boldsymbol{T}} \delta \boldsymbol{F'} \tag{36}$$

and then, according to the general solution of (30), given by

$$\delta \boldsymbol{T}_{\phi} = ([\boldsymbol{G^{\phi}_a}]^{\boldsymbol{T}})^{+} \delta \boldsymbol{T_a} + ([\boldsymbol{I}] - ([\boldsymbol{G^{\phi}_a}]^{\boldsymbol{T}})^{+} [\boldsymbol{G^{\phi}_a}]^{\boldsymbol{T}}) \varepsilon \tag{37}$$

the effort $(\delta \boldsymbol{T}_{\phi})$ at the total input locations is calculated only by using the first term of (37). In (37), $([\boldsymbol{G^{\phi}_a}]^{\boldsymbol{T}})^{+}$ denotes the pseudo-inverse solution of $[\boldsymbol{G^{\phi}_a}]^{\boldsymbol{T}}$. While the first-term of (37) denotes a minimum norm solution, the second-term represents a homogeneous solution creating an internal loading. Now, according to the compliance relation of (35), the joint angles are adjusted such that the force error can be eliminated.

In particular, the homogeneous solution offers chances of several subtasks. Though both the joint-based method and the object-based method can be considered in the control of the internal load state, we employ a joint-based load distribution scheme due to its applicability to general kinematic and actuation configuration [28].

C. Internal Force Control Algorithm

Typical dual-arm systems possess force redundancy. A number of redundant actuators enable several classes of internal force control. Owing to the general applicability of the joint-based load distribution schemes, we consider an approach which is based on imposing constraints on the joint space variables. Specifically, we consider constraints of the form [11], [28]

$$[\boldsymbol{G}(\phi]\delta\boldsymbol{T}_{\boldsymbol{\phi}} = \boldsymbol{\alpha} \tag{38}$$

where $[\boldsymbol{G}(\phi)] \in \Re^{(\boldsymbol{M_t}-\boldsymbol{M})\times\boldsymbol{M_t}}$, and $\boldsymbol{\alpha}$ is a known (time dependent) vector (recall that M is the mobility of the dual arm system). The constraints in (38), represented by the row of $\boldsymbol{G}$ and the corresponding elements in $\boldsymbol{\alpha}$, are independent of each other. This implies that $\boldsymbol{G}$ must have full rank. $\boldsymbol{G}$ and $\boldsymbol{\alpha}$ are to be selected according to the type of subtask to be performed and represent the criteria to be used in distributing the manipulator loads.

Assuming this has been accomplished, we wish to choose ε in (37) to satisfy the minimum norm solution as well as the additional subtask described in (38). Let $\boldsymbol{T'}$ is defined as the first-term of (37). Substitute (37) into (38) to obtain

$$[\boldsymbol{G}]\boldsymbol{T'} + [\boldsymbol{G}][[\boldsymbol{I}] - ([\boldsymbol{G}_{\boldsymbol{a}}^{\boldsymbol{\phi}}]^{\boldsymbol{T}})^{+}[\boldsymbol{G}_{\boldsymbol{a}}^{\boldsymbol{\phi}}]^{\boldsymbol{T}}]\varepsilon = \boldsymbol{\alpha} \tag{39}$$

or

$$[\boldsymbol{H}]\varepsilon = \boldsymbol{\alpha} - [\boldsymbol{G}]\boldsymbol{T'} \tag{40}$$

where

$$[\boldsymbol{H}] = [\boldsymbol{G}][[\boldsymbol{I}] - ([\boldsymbol{G}_{\boldsymbol{a}}^{\boldsymbol{\phi}}]^{\boldsymbol{T}})^{+}[\boldsymbol{G}_{\boldsymbol{a}}^{\boldsymbol{\phi}}]^{\boldsymbol{T}}]. \tag{41}$$

Now, the choice of

$$\varepsilon = [\boldsymbol{H}]^{+}(\alpha - [\boldsymbol{G}]\boldsymbol{T'}) \tag{42}$$

provides the minimum norm solution and the constraint equation (38). Here, $[\boldsymbol{H}]^{+}$ denotes the pseudo-inverse solution of $[\boldsymbol{H}]$.

There will be many different choices of possible $[G]$ in (38). In our experimental work, we utilize the internal loading to eliminate unwanted pitch motion which can be created by moment-unbalancing along the y (or pitch) direction during the sawing task (refer to Fig. 2). Now, we derive a force relationship between the mini-mum actuator coordinates and moment vector at the contact position. From (12), the angular velocity vector ω of the saw is obtained as

$$\omega = [\boldsymbol{J}_2]\dot{\phi}_{\boldsymbol{a}} \tag{43}$$

where $[J_2]$ denotes the matrix of dimension of 3×4, which is formed by collecting fourth, fifth, and sixth row vectors of $[\boldsymbol{G}_a^u]$. Now, from the duality relation between the force and velocity vectors, we have

$$\boldsymbol{T}_{\boldsymbol{a}} = [\boldsymbol{J}_2]^{\boldsymbol{T}}\boldsymbol{m} \tag{44}$$

where $\boldsymbol{m}$ denotes the moment vector at the contact point. Assuming that $[\boldsymbol{J}_2]$ is not singular, the moment vector is given as

$$\boldsymbol{m} = ([\boldsymbol{J}_2]^{\boldsymbol{T}})^{+}\boldsymbol{T}_{\boldsymbol{a}} = ([\boldsymbol{J}_2]^{\boldsymbol{T}})^{+}[\boldsymbol{G}_{\boldsymbol{a}}^{\boldsymbol{\phi}}]^{\boldsymbol{T}}\boldsymbol{T}_{\boldsymbol{\phi}} = [\boldsymbol{P}]\boldsymbol{T}_{\boldsymbol{\phi}}. \tag{45}$$

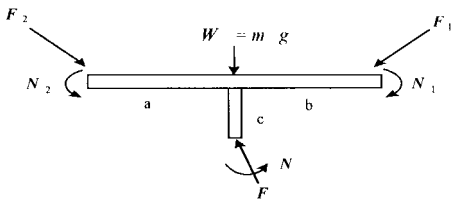

Fig. 5. Description of the grasped object.

Now, since we desire the moment about the y-axis to be kept zero regardless of the sawing motion, we decide $[G]$ and $\boldsymbol{\alpha}$ as

$$[\boldsymbol{G}] = [\boldsymbol{P}]_{2;}, \quad \boldsymbol{\alpha} = 0 \tag{46}$$

where $[\boldsymbol{P}]_{2;}$ denotes the second row of $[\boldsymbol{G}]$ and $\boldsymbol{\alpha}$ is a scalar. Besides the above example, more complex criteria involving groups of actuators can be possibly incorporated [11], [28].

Now, according to the compliance relation of (35), the joint angles are adjusted such that the force error can be eliminated.

The interaction force and moment between the dual arms and the environment can be measured using two F/T sensors attached to the end of each robot. Then, in a state of static equilibrium the relationship between the measured force/torque vectors and the interaction force/torque vector can be derived from Fig. 5, and is given as

$$\begin{bmatrix} F \\ N \end{bmatrix} = \begin{bmatrix} I & 0 & I & 0 \\ S_1 & I & S_2 & I \end{bmatrix} \begin{bmatrix} F_1 \\ N_1 \\ F_2 \\ N_2 \end{bmatrix} + \begin{bmatrix} \boldsymbol{W} \\ 0 \end{bmatrix} \tag{47}$$

where $\boldsymbol{W}$ denotes a gravity load vector and the matrix $\boldsymbol{S_i}$ denotes the mapping between the grasped force vector $\boldsymbol{F_i}$ of the ith robot and the moment $\boldsymbol{N}$ exerted by the environment on the grasped object. $\boldsymbol{N_i}$ denotes the moments vector exerted on the grasped object by the ith robot. $\boldsymbol{F_i}$ and $\boldsymbol{N_i}(i = 1, 2)$ are measured at the F/T sensor attached to the end of each robot.

V. Velocity Control for Sawing Task

In general, the sawing task is performed along a straight line in a plane. For this task, we need to control the translational motions along the x and y directions and the rotational motion about the z-axis.

A Jacobian which relates the velocity vector for those three motions to the velocity vector for minimum actuators is given as

$$\boldsymbol{v} = \begin{bmatrix} \dot{\boldsymbol{x}} \\ \dot{\boldsymbol{y}} \\ \omega_z \end{bmatrix} = [\boldsymbol{J}_3]\dot{\phi}_{\boldsymbol{a}} \tag{48}$$

where $[\boldsymbol{J}_3]$ denotes a matrix of dimension of 3×4, formed by collecting the first, second, and the sixth rows of $[\boldsymbol{G}_{\boldsymbol{a}}^{\boldsymbol{u}}]$.

For a given trajectory of the saw, $\dot{\boldsymbol{\phi}}_{\boldsymbol{a}}$ is obtained according to

$$\dot{\boldsymbol{\phi}}_{\boldsymbol{a}} = [\boldsymbol{J}_3]^{+}\boldsymbol{v} \tag{49}$$

where $[\boldsymbol{J}_3]^{+}$ denotes the pseudo-inverse of $[\boldsymbol{J}_3]$, and then the velocity of all joints are determined from (9). Every joint except the passive joint is driven by each joint motor. Though only the minimum actuators can generate the motion, the

TABLE I
KINEMATIC PARAMETERS OF PT200V ROBOT

Parameter / Joint	Link Length a_i	Twist Angle α_i	Offset d_i	Rot Angle θ_i
1	0 m	90°	0.2 m	θ_1
2	0.2 m	0°	0 m	θ_2
3	0.25 m	0°	0 m	θ_3
4	0.25 m	90°	0 m	θ_4
5	0 m	0°	0.065 m	θ_5

TABLE II
KINEMATIC PARAMETERS OF SCARA ROBOT

Parameter / Joint	Link Length a_i	Twist Angle α_i	Offset d_i	Rot Angle θ_i
1	0.367 m	0°	0 m	θ_1
2	0.233 m	0°	0 m	θ_2
3	0 m	0°	d_3 m	0
4	0 m	0°	0 m	θ_4
5	0.3 m	90°	0 m	θ_5

TABLE III
INITIAL CONFIGURATION OF OUR TWO-ARM SYSTEM

Robot / Initial Angle	PT200V Robot	SCARA Robot
θ_1	-9.21°	58.9°
θ_2	20.75	85.46°
θ_3 or d_3	34.89°	0.17 m
θ_4	24.4°	-54.39°
θ_5	9.21°	0.0°

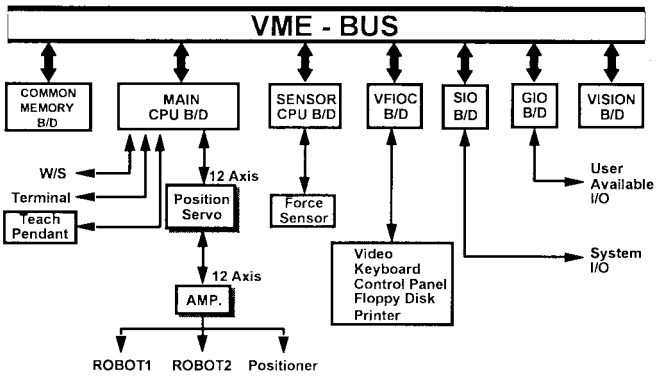

Fig. 6. Hardware architecture of the multirobot controller.

redundant joints take the role of load sharing for motion. In that sense, the passive joint does not participate in the load sharing, but just moves dependently of the minimum joints due to the nature of the closed kinematic chain of the two-arm system. A simple PID velocity controller is employed to compensate for the velocity error and also to obtain a good transient response of the planned velocity.

VI. EXPERIMENTAL RESULTS

Sawing experiments have been performed by using two arms with an additional passive joint; one four-axis SCARA robot and one 5-axis articulated industrial robot manipulator (PT200V). Kinematic parameters for each robot are described in Tables I and II, respectively. Table III includes the initial configuration of the dual arm system. In this configuration, the mobility is four according to equation (1). Therefore, the four axes from the base of PT200V robot are chosen as the independent joint set, although there are many potential independent joint sets.

Each robot is equipped with a force sensor at its end-point. The interaction force and moment between the dual arms and the environment can be measured using two F/T sensors attached to the end of each robot. Our control scheme is written in C-language and tested in our prototype dual robot controller [7] as shown in Fig. 6. Two 32-bit microprocessor boards (FORCE30 [24], KVME040) are used. One board is a main CPU board for trajectory generation, each joint control, user interface, etc. The other one is employed as a sensor CPU board for raw sensor data acquisition from sensors, sensor data handling, transmitting control data to the main CPU board, etc.

According to time analysis, motion generation costs 30 ms and user interface needs 34 ms. On the other hand, the force control requires 64 ms. This large sampling time in the force control is due to computation time of our proposed force control algorithm. In total, our sampling time is 64 ms (15 Hz). The rise time of the force response is about 1 s. In general, the speed of the sawing task is not that fast. The maximum experimental speed in our sawing task is given 1 Hz. Since our force control algorithm is running 15 times faster than the operating speed, we expect that we can obtain a good force response.

Fig. 6 shows the hardware architecture of our multirobot controller.

Note that satisfactory performances can be obtained only under the condition that the actual environmental stiffness value is exactly given by an operator. In most practical cases, exact environmental stiffness values are not known in advance and thus they should be automatically measured or estimated as a robot contacts with unknown environments. In order to estimate the unknown or changing magnitude of the environmental stiffness, many researchers have proposed several sophisticated approaches [4], [8], [12], [19] which employ robot dynamics and adaptation methods. In this work, we estimate the magnitude of the environmental

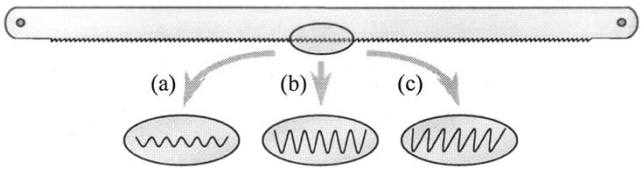

Fig. 7. Shape of saw blades. (a) Symmetric saw blade with tooth depth less than 0.1 mm. (b) Symmetric saw blade with tooth depth 0.3 mm. (c) Asymmetric saw blade with tooth depth 0.3 mm.

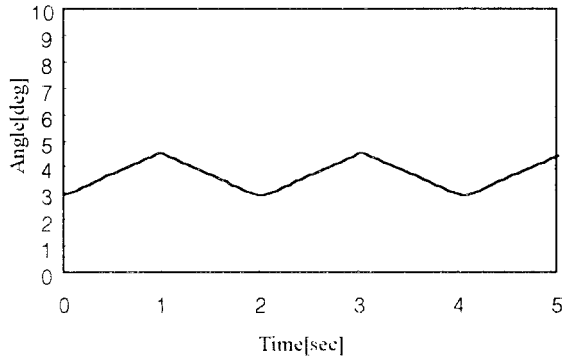

Fig. 8. Roll motion when an additional passive joint is not included.

stiffness, experimentally, by measuring the force for an induced displacement against the environment [6]. The stiffness magnitude of the object to be sawn has been experimentally measured as 35000 N/m. In fact, our measured stiffness represents the combination of environment stiffness, robot arm stiffness, and the force/torque sensor stiffness.

Performances of the sawing task can be influenced by several factors. We consider three important factors; shape of saw blades given in Fig. 7, sawing speed, and vertical force. In the sawing task, a force along the vertical direction of the environment surface is required not to loose the contact with the environment. However, applying a large vertical force is not desirable since the driving force of the saw should be increased proportional to the magnitude of the friction force which is the product of the vertical force and friction coefficient of the sawn material. Therefore, the magnitude of the vertical force will be decided according to the strength and the roughness of the material to be sawn. In our experimentation, we consider two different vertical forces (i.e., 5 and 10 Newton). The motion of the saw is controlled to have periodic motion in the x-direction. We also considered two different sawing speeds (i.e., 0.1 and 0.2 m/s).

Initially, we perform sawing task with the blade type (a) of Fig. 7 under the conditions of 0.1 m/s sawing speed and 5 N vertical force. Fig. 8 shows the roll motion (rotational motion about the z-axis of Fig. 2) when the additional passive joint is not included. This roll motion is not desirable since it keeps the saw from following a straight-line motion. On the other hand, Fig. 9 shows that the unwanted roll motion can be eliminated by including a passive joint to the system. A small perturbation is observed at each moment that the motion of the saw is reversed. This may be due to the backlash existing in the two-arm system. Also, an internal load control to suppress

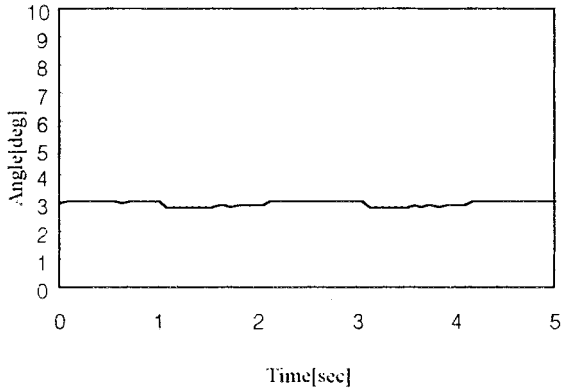

Fig. 9. Roll motion when an additional passive joint is included.

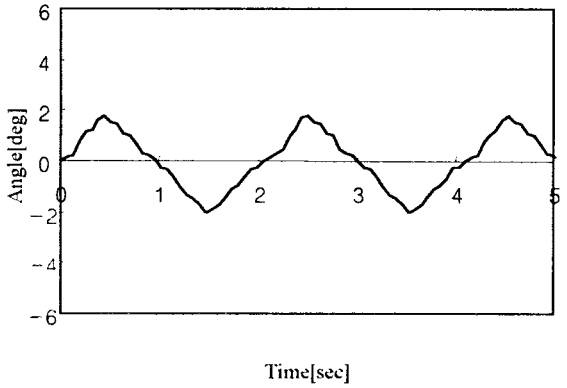

Fig. 10. Pitch motion without consideration of the internal load control.

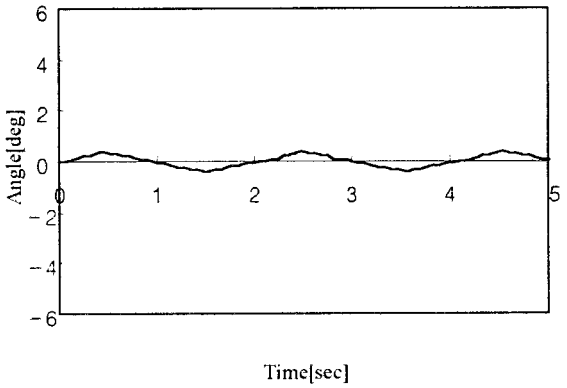

Fig. 11. Pitch motion with consideration of the internal load control.

an unwanted pitch motion (rotational motion about the y-axis of Fig. 2) have been considered. Without consideration of the internal load control algorithm derived in the Section IV, a periodic pitch motion occurs in the sawing task, as shown in Fig. 10. By using the internal load control algorithm, the pitch motion can be notably reduced as shown in Fig. 11. The remaining pitch motion of Fig. 11 may be caused by the dynamic motion of the saw. Also, Figs. 12 and 13 demonstrate the force and velocity responses for our proposed control scheme. The rise time for both responses is about 1 s and the transient responses look stable. We conclude that the saw

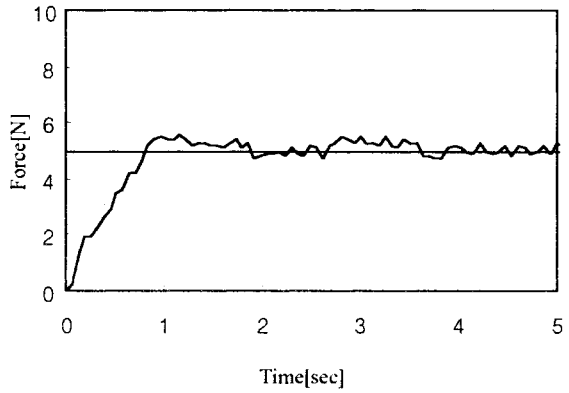

Fig. 12. Force control in the sawing task [blade type (a)].

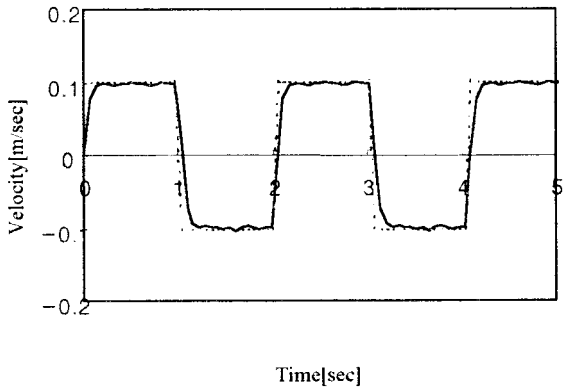

Fig. 13. Velocity control in the sawing task [blade type (a)].

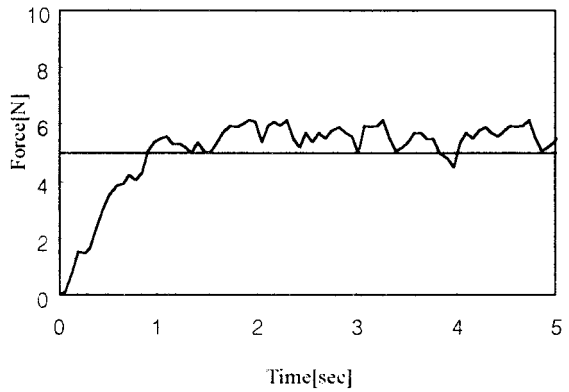

Fig. 14. Force control in the sawing task [blade type (b)].

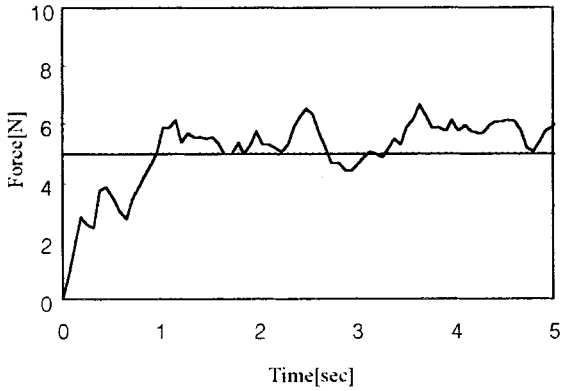

Fig. 15. Force control in the sawing task [blade type (c)].

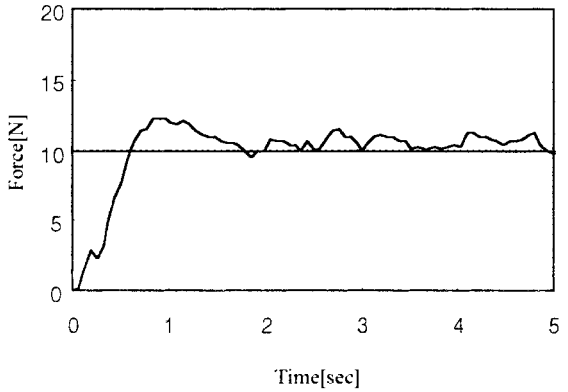

Fig. 16. Force control in the sawing task [blade type (a)].

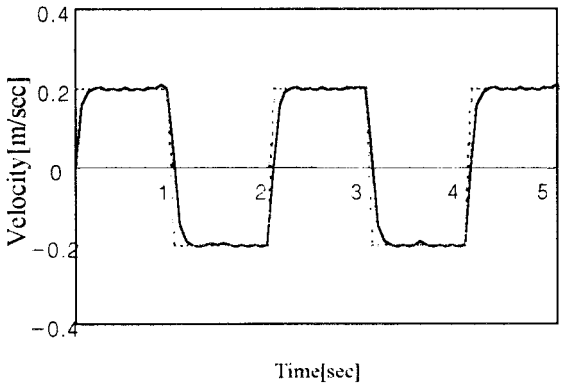

Fig. 17. Velocity control in the sawing task [blade type (a)].

follows the desired trajectories satisfactorily in both velocity- and force-levels.

In order to show the effectiveness of the proposed algorithms, we perform several experimentation considering other factors. Figs. 14 and 15 demonstrate the vertical force responses under the same speed and vertical-force conditions when using two, different saw blades [i.e., type (b) and type (c)] given in Fig. 7. Moreover, Figs. 16 and 17 demonstrate the force and velocity responses for the blade type a, under the conditions of 0.2 m/s sawing speed and 10 N vertical force, respectively. As the magnitude of the vertical force, the speed of the sawing task, and the thickness or roughness of the saw increase, we could observe that the sawing performances deteoriorate relatively. Nonetheless, the overall sawing performances are still satisfactory.

VII. Conclusion

In this work, we propose a hybrid control method for sawing task using two arms with an additional passive joint. The proposed scheme is able to treat the kinematics, dynamics, and control of a two-arm system with general kinematic structure,

and it is different from other acceleration-based approach in the sense that our hybrid control method is based on a Jacobian and an internal kinematics for a single closed-kinematic chain of the two arms to reflect the nature of the position-controlled industrial manipulator. Also, the proposed scheme is not only able to operate the system even if a passive joint exists, but also able to utilize the internal loads for useful applications such as pitch motion control. We experimentally show that by inserting a passive joint to the two-arm system, the proposed control scheme is able to keep the system form the unwanted roll motion and unwanted pitch motion in the sawing task as well as yield a satisfactory performance in the velocity and force responses. To show the effectiveness of the proposed algorithms, we perform experimentation under several, different conditions for saw, such as three saw blades, two sawing speeds, and two vertical forces.

Basically, our work suggests a hybrid control algorithm for the sawing task, which has been quite successful within the allowable range of hardware capability. However, in reality, the sawing speed could be much faster than those in our experimental work, the saw blades could be much thicker, and the applied vertical force could be much larger. In order to overcome those difficulties, we need to enhance the performances of our controller (i.e., increase the sampling time by employing parallel computation method or using much faster processor such as DSP board), which is our future work.

REFERENCES

[1] M. T. Mason, "Compliance and force control for computer controlled manipulators," *IEEE Trans. Syst., Man, Cybern.*, vol. SMC-11, pp. 418–432, 1981.

[2] M. W. Raibert and J. J. Craig, "Hybrid position/force control of manipulators," *Int. J. Dyn. Syst. Meas. Contr.*, vol. 102, pp. 120–133, 1981.

[3] B.-J. Yi, I. H. Suh, and S.-R. Oh, "Analysis of a 5-bar finger mechanism having redundant actuators with applications to stiffness and frequency modulations," in *Proc. IEEE Int. Conf. Robot. Automat.*, Albuquerque, NM, 1997, pp. 759–765.

[4] W. S. Lu and Q. H. Meng, "Impedance control with adaptation for robotic manipulation," *IEEE J. Robot. Automat.*, vol. 7, pp. 308–415, June 1991.

[5] B.-J. Yi, S.-R. Oh, I. H. Suh, and B.-J. You, "Synthesis of frequency modulator via redundant actuation: The case for a five-bar finger mechanism," in *Proc. IEEE/RSJ Conf. Intell. Robot Syst.*, Grenoble, France, 1997, pp. 1098–1104.

[6] I. H. Suh, K. S. Eom, H. J. Yeo, and S. R. Oh, "Fuzzy adaptation force control of industrial robot manipulators with position servos," *Int. J. Mechatron.*, vol. 5, no. 8, pp. 899–918, 1995.

[7] I. H. Suh, H. J. Yeo, T. W. Kim, and S. R. Oh, "A control system for multiple-robot manipulators; design and implementation," in *Proc. Int. Conf., ISRAM*, vol. 5, pp. 279–285, 1994.

[8] X. Cui and K. G. Shin, "Direct control and coordination using neural networks," *IEEE Trans. Syst., Man, Cybern.*, vol. 23, pp. 686–697, 1993.

[9] J. M. Tao, J. Y. S. Luh, and Y. F. Zheng, "Compliant coordination control of two moving industrial robots," *IEEE J. Robot. Automat.*, vol. 6, pp. 322–330, June 1990.

[10] M. Uchiyama *et al.*, "Adaptive load sharing for hybrid controlled two cooperative manipulators," in *Proc. IEEE Int. Conf. Robot. Automat.*, Sacramento, CA, 1991, pp. 986–991.

[11] B.-J. Yi and R. A. Freeman, "Geometric analysis of antagonistic stiffness in redundantly actuated parallel mechanisms," *Int. J. Robot. Syst.*, vol. 10, no. 5, pp. 581–603, 1993.

[12] M. Pelletier and L. K. Daneshmend, "An adaptive compliance motion controller for robot manipulators based on damping control," in *Proc. IEEE Int. Conf. Robot. Automat.*, 1990, pp. 1060–1065.

[13] H. Seraji, "Adaptive admittance control: An approach to explicit force control in compliant motion," in *Proc. IEEE Int. Conf. Robot. Automat.*, San Diego, CA, 1994, pp. 2705–2712.

[14] T. Yoshikawa and X. Z. Zheng, "Coordinated dynamic hybrid position/force control for multiple robot manipulators handling one constrained object," *Int. J. Robot. Res.*, vol. 12, no. 3, pp. 219–230, 1993.

[15] C. A. Derventzis and E. J. Davison, "Robust motion/force control of cooperative multi-arm systems," in *Proc. IEEE Int. Conf. Robot. Automat.*, 1992, pp. 2230–2337.

[16] Y. R. Hu, A. A. Goldenberg, and C. Zhou, "Motion and force control of coordinated robots during constrained motion tasks," *Int. J. Robot. Res.*, vol. 14, no. 4, pp. 351–365, 1995.

[17] B.-J. Yi and R. A. Freeman, "Feedforward spring-like impedance modulation in human arm models," in *Proc. IEEE Int. Conf. Robot. Automat.*, Nagoya, Japan, 1995, pp. 654–661.

[18] K. Kosuge *et al.*, "Decentralized control of robots for dynamic coordination," in *Proc. IEEE/RSJ Int. Conf. Intell. Robots Syst.*, 1995, pp. 76–81.

[19] I. H. Suh *et al.*, "Fuzzy rule based position/force control of industrial manipulators," in *Proc. IEEE/RSJ Int. Conf. Intell. Robots Syst.*, Osaka, Japan, 1991, pp. 1617–1622.

[20] S. Fujii and S. Kurono, "Coordinated computer control of a pair if manipulators," in *Proc. Int. Conf. 4th IFTIMM World Congr.*, 1975, pp. 411–417.

[21] R. G. Bonitz and T. C. Hsia, "Internal force-based impedance control for cooperating manipulators," *IEEE J. Robot. Automat.*, vol. 12, pp. 78–89, Dec. 1996.

[22] M. Uchiyama and P. Dauchez, "A symmetric hybrid position/force control scheme for the coordination of two robots," in *Proc. IEEE Int. Conf. Robot. Automat.*, Philadelphia, PA, 1988, pp. 350–356.

[23] Y. F. Zheng and J. Y. S. Luh, "Optimal load distribution for two industrial robots handling a single object," in *Proc. IEEE Int. Conf. Robot. Automat.*, Philadelphia, PA, 1988, pp. 344–349.

[24] *CPU-30 User's Manual*, Force Computers, Inc., Germany, 1991.

[25] H. J. Kang, B.-J. Yi, W. Cho, and R. A. Freeman, "Constraint embedding approaches for general closed-chain system dynamics in terms of a minimum coordinate set," in *Proc. Conf. ASME 21st Mechanism*, Chicago, IL, 1990, vol. DE-24, pp. 125–132.

[26] B.-J. Yi, S.-R. Oh, I. H. Suh, and W. K. Kim, "Frequncy modulation in anthropomorphic robots with kinematic and force redundancies," in *Proc. IEEE Int. Conf. Robot. Automat.*, Leuven, Belgium, 1998, pp. 2697–2702.

[27] J. H. Lee, B.-J. Yi, S.-R. Oh, and I. H. Suh, "Optimal design of a five-bar finger with redundant actuation," in *Proc. IEEE Int. Conf. Robot. Automat.*, Leuven, Belgium, 1998, pp. 2068–2074.

[28] I. D. Walker, R. A. Freeman, and S. I. Marcus, "Analysis of motion and internal loading of objects grasped by multiple cooperating manipulators," *Int. J. Robot. Res.*, vol. 10, no. 4, pp. 396–409, 1991.

[29] H. J. Yeo, S. J. Lee, I. H. Suh, B. J. Yi, and S. R. Oh, "External force control using cooperating two arms with general kinematic structures," *Proc. IEEE Int. Conf. Robot Human Commun.*, Tokyo, Japan, 1996, pp. 388–394.

[30] H. J. Yeo, I. H. Suh, B. J. Yi, S. R. Oh, and B. H. Lee, "A closed-chain Jacobian-based hybrid control for two cooperating arms with a passive joint: An application to sawing task," in *Proc. IEEE Int. Conf. Robot. Automat.*, Albuquerque, NM, 1997, pp. 1793–1800.

[31] K. H. Hunt, *Kinematic Geometry of Mechanisms.* New York: Clarendon, 1978.

[32] C. Gosselin and J. Angeles, "Singularity analysis of closed-loop kinematic chains," *IEEE J. Robot. Automat.*, vol. 6, pp. 281–290, June 1990.

[33] S. Tzafetas, "Incremental fuzzy expert PID control," *IEEE J. Ind. Electron.*, vol. 15, pp. 15–30, 1979.

Hee-Joo Yeo received the B.S., M.S., and Ph.D. degrees in electronics engineering from Hanyang University, Korea, in 1988, 1990, and 1997, respectively.

Since 1997, he has been with the Department of Electronics Engineering, Daejin University, Korea, where he is an Assistant Professor. His research interests include motor control, sensor-based control of robot manipulators, coordination control of multiple robot arms, machine vision, fuzzy logics, and neural networks.

Il Hong Suh (M'89) was born in Seoul, Korea. He received the B.S. degree in electronics engineering from Seoul National University, Korea, in 1977 and the M.S. and Ph.D. degrees in electrical engineering from the Korea Institute of Science and Technology (KAIST), Seoul, in 1979 and 1982, respectively.

From 1982 to 1985, he was a Senior Research Engineer at the Technical Center of Daewoo Heavy Industries, Ltd., Inchon, Korea, where he was involved in the research works on machine vision and the development of the Daewoo NOVA10 robot controller. From 1985 to 1986, he joined the Systems Control Laboratory, KAIST, as a part-time Research Fellow for an automation-related Korea National Project. In 1987, he was a Visiting Research Fellow at the Robotics Division, CRIM, University of Michigan, Ann Arbor. Since 1985, he has been with the Department of Electronics Engineering, Hanyang University, Korea, where he is a Professor. He has served as Vice Dean of Academic Affairs, Ansan Campus, Hanyang University, since 1996. His research interests include sensor based control of robot manipulators, coordination of multiple robot arms, and robust control, intelligent control involving fuzzy logics, and neural networks.

Byung-Ju Yi (M'89) received the B.S. degree from the Department of Mechanical Engineering, Hanyang University, Seoul, Korea in 1984, and the M.S. and Ph.D. degrees from the Department of Mechanical Engineering, University of Texas at Austin, in 1986 and 1991, respectively.

From January 1991 to August 1992, he was a Post Doctoral Fellow with the Robotics Group, University of Texas at Austin. From September 1992 to February 1995, he was an Assistant Professor in Department of Mechanical and Control Engineering, Korea Institute of Technology and Education (KITE), Chonan, Chungnam, Korea. In March 1995, he joined Hanyang University, Ansan, Kyungki-Do, Korea as an Assistant Professor in the Department of Control and Instrumentation Engineering. He is an Associate Professor with the Department of Electrical and Computer Engineering, Hanyang University. His research interests include design, control, and application of multiple arms, parallel manipulator, and anthropomorphic manipulator systems.

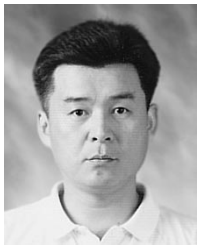

Sang-Rok Oh (S'80–M'91) received the B.S. degree in electronic engineering from Seoul National University, Seoul, Korea, in 1980, and the M.S. and Ph.D. degrees in electrical and electronic engineering from the Korea Advanced Institute of Science and Technology (KAIST), Daeduk, Korea, in 1982 and 1987, respectively.

He worked as a Research Associate at the Systems Control Laboratory, KAIST, for ten months in 1987, conducting the design and implementation of multiprocessor-based automatic assembly machine for micro electronic components and robotic control system for multilegged locomotion. In 1988, he joined the Korea Institute of Science and Technology (KAST), Seoul, Korea, and is a Principal Research Engineer at the Intelligent System Control Research Center, KAST. He was a Visiting Scientist at the T. J. Watson Research Center, IBM, Yorktown Heights, NY, from 1991 to 1992, conducting precision assembly using the magnetically levitated robot wrist. He also worked as a Visiting Scientist at the Mechanical Engineering Laboratory, Tsukuba, Japan, for three months in 1995, investigating the area of mobile manipulation system. His research interests include intelligent control of robot manipulators, mobile manipulation, multifingered robotic hand, and service robots.

Dr. Oh is a member of the Korea Institute of Electrical Engineering, the Korea Fuzzy Logic and Intelligent Systems Society, and the Institute of Control, Automation, and System Engineering, Korea.